we define the numerical flux by

$$\Phi^{DM}(U_l, U_r) = F^{DM}[V_{l,r}(0,t)]$$

Algebraic Expression of the Numerical Flux

For $i \in S$, the Hermite interpolation polynomial $p_i(w)$ introduced previously is defined by

$$p_i(w) = aw^3 + bw^2 + cw$$

with

$$a = \frac{\lambda_i(U_i) + \lambda_i(U_{i-1}) - 2\lambda_i^R}{\alpha_i^2}$$

$$b = \frac{3\lambda_i^R - 2\lambda_i(U_{i-1}) - \lambda_i(U_i)}{\alpha_i}$$

$$c = \lambda_i(U_{i-1})$$

The modified numerical flux has the expression

$$\Phi^{DM}(U_l, U_r) = F(U_l) + \sum_{i \notin S,\ \lambda_i^R < 0} \lambda_i^R \alpha_i R_i(U_l, U_r) + \sum_{i \in S} p_i(\theta_i^*) R_i(U_l, U_r)$$

where

$$\theta_i^* = \frac{-\lambda_i(U_{i-1}) \cdot \alpha_i}{3\lambda_i^R - 2\lambda_i(U_{i-1}) - \lambda_i(U_i) + \sqrt{[3\lambda_i^R - \lambda_i(U_i) - \lambda_i(U_{i-1})]^2 - \lambda_i(U_{i-1})\lambda_i(U_i)}}$$

is the argument of the unique extremum of g_i between 0 and α_i.

Remark

Note that when α_i is positive, $g_i(\theta_i^*)$ is the unique minimum of the polynomial p_i between 0 and α_i and we have

$$g_i(\theta_i^*) \le 0$$

$$g_i(\theta_i^*) \le \lambda_i^R \alpha_i$$

It is easy to see that our numerical flux can be written in a centered form that makes the added numerical viscosity explicit:

$$\Phi^{DM}(U_l, U_r) = \Phi^R(U_l, U_r) + \sum_{i \in S} \sup\,[g_i(\theta_i^*);\ g_i(\theta_i^*) - \lambda_i^R \alpha_i] R_i(U_l, U_r)$$

where $\Phi^R(U_l, U_r)$ is the classical Roe flux.[1]

Theorem: Convergence to the Unique Entropy Solution

Let f be a convex scalar flux and u^0 initial data in $L^\infty(\boldsymbol{R}) \cap BV(\boldsymbol{R})$. The semidiscrete numerical scheme:

$$\frac{du_j}{dt} = -\frac{1}{h}[\Phi^{DM}(u_j, u_{j+1}) - \Phi^{DM}(u_{j-1}, u_j)]$$

with

$$u_j(0) = \frac{1}{h}\int_{(j-1/2)h}^{(j+1/2)h} u^0(x)\,dx$$

where h is the mesh step, converges to the unique entropy solution of Eq. (1) with initial data u^0 (see proof in Ref. 4).

Conclusions

We have proposed a nonparameterized approach to entropy enforcement for Roe-type schemes. It is based on the exact resolution of a Riemann problem associated with a Hermite interpolation of the physical flux. In the scalar convex case, we have proved convergence of the method of lines to the unique entropy solution. Numerical results[5] for the Euler equations extend the conclusions of the scalar case.

References

[1]Roe, P. L., "Approximate Riemann Solvers, Parameter Vectors, and Difference Schemes," *Journal of Computational Physics*, Vol. 43, No. 2, 1981, pp. 357–372.

[2]Harten, A., and Hyman, J. M., "Self-Adjusting Grid Methods for One-Dimensional Hyperbolic Conservation Laws," *Journal of Computational Physics*, Vol. 50, No. 1, 1983, pp. 235–269.

[3]Roe, P. L., "Some Contributions to the Modeling of Discontinuous Flow," Modeling of Discontinuous Flow," *Lectures in Applied Mathematics*, edited by Engquist, Osher, and Sommerville, Vol. 22, American Mathematical Society, Providence, RI, 19085, pp. 163–193.

[4]Dubois, F., and Mehlman, G., "A Non-Parameterized Entropy Correction for Roe's Approximate Riemann Solver," CMAP Rept. 248, Ecole Polytechnique, Palaiseau, France, 1991.

[5]Mehlman, G., Thivet, F., Candel, S., and Dubois, F., "Computation of Hypersonic Flows with a Fully Coupled Implicit Solver and an Extension of the CVDV Model for Thermochemical Relaxation," GAMNI Hypersonic Workshop, Antibes, France, April 1991 (to be published).

Shock Oscillation in Two-Dimensional, Inviscid, Unsteady Channel Flow

Shen-Min Liang* and Chou-Jiu Tsai†
National Cheng Kung University, Tainan, Taiwan 70101, Republic of China

Introduction

UNSTEADY transonic channel flows with shock waves, such as inlet flows for air-breathing engines, have received considerable attention. Unsteadiness in the flow may arise from pressure pulses caused by combustion or ignition far downstream of the channel. The avoidance of these unwanted, unsteady flow phenomena is desirable, and understanding of their flow structures would be beneficial for aircraft design.

Methods for studying this problem were primarily the asymptotic expansion methods,[1,2] numerical methods,[3-5] or both.[6] Richey and Adamson[1] have found that, in the slowly time-varying regime, the amplitude of shock oscillation is of order ϵ if the imposed pressure fluctuation has amplitude of order ϵ^2 and period of order ϵ^{-1}, where ϵ denotes a small parameter used to measure the difference between the flow velocity and the sound speed. Adamson et al.[2] have found that small changes in imposed pressures can cause large-amplitude

Received Nov. 4, 1991; revision received July 18, 1992; accepted for publication July 21, 1992.

*Associate Professor, Institute of Aeronautics and Astronautics. Member AIAA.

†Graduate Student, Institute of Aeronautics and Astronautics.

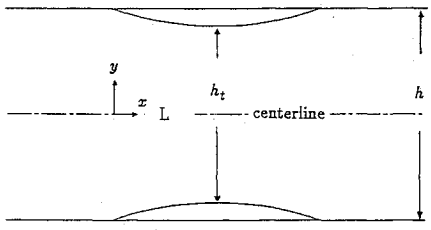

Fig. 1 Sketch of a channel and its coordinates.

shock wave motion. Liou and Coakley[3] used the Reynolds-averaged Navier-Stokes equations to simulate forced and self-excited oscillations of transonic flows in two-dimensional diffusers. Hseih[4] studied downstream boundary effects on the frequency of self-excited oscillations in transonic diffusers. Bölcs et al.[5] investigated inviscid unsteady flows through nozzles and noted that the nozzle geometry was an important parameter. Biedron and Adamson[6] presented a unified solution containing fundamentally unsteady and quasisteady flows. They employed asymptotic and numerical methods to study the effect of the boundary layer thickness on the shock wave motion.

In this study the objective is to compare the difference of forced shock oscillations between the two-dimensional and one-dimensional channel flows with different values of channel expansion ratio h/h_t. Define the parameter τ as the difference between the channel exit area h and the throat area h_t divided by the throat area h_t, i.e., $\tau \equiv h/h_t - 1$, as shown in Fig. 1. The corresponding maximum area change in the channel is $\tau/(\tau + 1)$. Generally speaking, asymptotic methods are valid only for small values of τ compared to 1; for large values of τ, numerical methods are called for. In addition to the parameter τ, the influence of amplitude and frequency of the imposed pressure on the shock movement is explored extensively. The numerical results are obtained by solving the Euler equations by using a time-accurate scheme.[7] Because of space limitations, only some prominent flow characteristics are reported.

Mathematical Formulation and Numerical Method

Mathematical Formulation

By neglecting viscous effects, the equations governing the transonic unsteady channel flow are the Euler equations

$$\partial_t U + \partial_x F(U) + \partial_y G(U) = 0 \tag{1}$$

where

$$U = \begin{bmatrix} \rho \\ \rho u \\ \rho v \\ E \end{bmatrix}, \quad F = \begin{bmatrix} \rho u \\ \rho u^2 + p, \\ \rho uv \\ (D + p)u \end{bmatrix}, \quad G = \begin{bmatrix} \rho v \\ \rho uv \\ \rho v^2 + p \\ (E + p)v \end{bmatrix}$$

and ρ is the density, (u,v) the velocity components in the Cartesian coordinates, p the pressure, $E = \rho[e + (u^2 + v^2)/2]$ the total energy per unit volume, and e the specific internal energy. Assuming that the flow is a perfect gas with a constant specific heat ratio γ, the equation of state is

$$(\gamma - 1)[E - 0.5\rho(u^2 + v^2)] \tag{2}$$

For easy use of the boundary condition on the wall, body fitted coordinates (ξ, η) are used. After the coordinate transformation, Eq. (1) can be expressed by

$$\partial_t \hat{U} + \partial_\xi \hat{F} + \partial_\eta \hat{G} = 0 \tag{3}$$

where $\hat{U} = U/J, \hat{F} = (\xi_x F + \xi_y G)/J, \hat{G} = (\eta_x F + \eta_y G)/J$, and $J = \xi_x \eta_y - \xi_y \eta_x$, the Jacobian representing the area of a control element.

Numerical Method

Let Δt be the time step and the grid spacing be denoted by $\Delta\xi$ and $\Delta\eta$ such that $\xi = j\Delta\xi$ and $\eta = k\Delta\eta$. Also, let $\lambda^\xi = \Delta t/\Delta\xi$ and $\lambda^\xi = \Delta t/\Delta\eta$. A two-parameter family of explicit and implicit total variation diminishing (TVD) type algorithms for Eq. (3) in a finite volume approach can be written as[8]

$$\begin{aligned} &\Delta\hat{U}^n_{j,k} + \frac{\lambda^\xi\theta}{1+\omega}[\tilde{F}^{n+1}_{j+1/2,k} - \tilde{F}^{n+1}_{j-1/2,k}] \\ &+ \frac{\lambda^\eta\theta}{1+\omega}[\tilde{G}^{n+1}_{j,k+1/2} - \tilde{G}^{n+1}_{j,k-1/2}] \\ &= \frac{(1-\theta)\lambda^\xi}{1+\omega}[\tilde{F}^{n}_{j+1/2,k} - \tilde{F}^{n}_{j-1/2,k}] \\ &- \frac{(1-\theta)\lambda^\eta}{1+\omega}[\tilde{G}^{n}_{j,k+1/2} - \tilde{G}^{n}_{j,k-1/2}] + \frac{\omega}{1+\omega}\Delta\hat{U}^{n-1}_{j,k} \end{aligned} \tag{4}$$

where $\Delta\hat{U}^n_{j,k} = \hat{U}^{n+1}_{j,k} - \hat{U}^n_{j,k}$. The functions $\tilde{F}_{j+1/2,k}$ and $\tilde{G}_{j,k+1/2}$ are the numerical fluxes in the ξ and η directions evaluated at $(j + 1/2, k)$ and $(j, k + 1/2)$, respectively. The scheme is second order in time if $\theta = \omega + 1/2$ and is first order otherwise. In this note, we set $\omega = 0$ and $\theta = 1$ for steady-state calculation and $\theta = 1/2$ for unsteady flow calculation. The spatial accuracy of Eq. (4) depends on the numerical flux. For example, Harten[9] defined $\tilde{F}_{j+1/2,k}$ as

$$\tilde{F}_{j+1/2,k} = \frac{1}{2}[\tilde{F}_{j+1,k} + \tilde{F}_{j,k} + R_{j+1/2,k}\Phi_{j+1/2,k}/J_{j+1/2,k}] \tag{5}$$

where R denotes the matrix consisting of the right eigenvectors of the Jacobian $\partial\tilde{F}/\partial\hat{U}$ and Φ the column vector composed of the elements denoted by ϕ^l:

$$\begin{aligned} \phi^l_{j+1/2,k} &= \frac{1}{2}\psi(a^l_{j+1/2,k})(g^l_{j,k} + g^l_{j+1,k}) \\ &- \psi(a^l_{j+1/2,k} + r^l_{j+1/2,k})\alpha^l_{j+1/2,k} \end{aligned} \tag{6}$$

Here the function ψ is an entropy correction[9] given by

$$\psi(z) = \begin{cases} |z|, & |z| \geq \delta; \\ (z^2 + \delta^2)/2\delta, & |z| < \delta \end{cases} \tag{7}$$

In this study, the parameter δ is set to be 1/8. Note that the variable $a^l_{j+1/2,k}$ in Eq. (6) denotes the characteristic speed for the Jacobian $\partial\tilde{F}/\partial\hat{U}$ and is evaluated by the Roe average[10] at the interface between $\hat{U}_{j,k}$ and $\hat{U}_{j+1,k}$, and note that the variable $r^l_{j+1/2,k}$ is the characteristic speed for the limiter $g_{j+1/2,k}$, which is defined as

$$r^l_{j+1/2,k} = \begin{cases} \frac{1}{2}\psi(a^l_{j+1/2,k})(g^l_{j+1/2,k} - g^l_{j,k})/\alpha^l_{j+1/2}, & \alpha^l_{j+1/2,k} \neq 0; \\ 0, & \alpha^l_{j+1/2,k} = 0 \end{cases} \tag{8}$$

In Eq. (8), the limiter $g^l_{j,k}$ is defined as $g^l_{j,k} = minmod(\alpha^l_{j-1/2,k}, \alpha^l_{j+1/2,k})$, and $\alpha^l_{j+1/2,k}$ are the characteristic variables, i.e., the elements of $R^{-1}_{j+1/2,k}(\hat{U}_{j+1,k} - \hat{U}_{j,k})$. The *minmod* function of two or more arguments is equal to the smallest number in absolute value if all of the arguments are of the same sign, or the function is equal to zero if any two arguments are of opposite sign. The numerical flux in the η direction $\tilde{G}_{j,k+1/2}$ is constructed in the same fashion. Later, Yee[11] modified the Harten scheme by replacing $g_{j,k} + g_{j+1,k}$ by *minmod* $(\alpha_{j-1/2,k}, \alpha_{j+1/2,k}, \alpha_{j+3/2,k})$. The authors found that a further modification on the Yee scheme by replacing $g_{j,k} + g_{j+1,k}$ as *minmod* $(\alpha_{j-3/2,k}, \alpha_{j-1/2,k}, \alpha_{j+1/2,k})$ can lead to an accurate scheme with fast convergence for steady-state flow calculation,[7] since more appropriate weighting on the initial data is used in the scheme. Finally, approximate factorization and linearization are employed for solving the discretized equation.[12]

Boundary Conditions

On Body Surfaces

The boundary condition on the body surface is the tangency condition. The tangential contravariant velocity components on the boundary are extrapolated from interior points, as suggested by Hung.[13] Using the known p_η, at the cell centers next to the wall, the pressure on the body surface is computed from the normal momentum equation:

$$\rho u(\eta_x u_\xi + \eta_y v_\xi) = -[(\xi_x \eta_x + \xi_y \eta_y)p_\xi + (\eta_x^2 + \eta_y^2)p_\eta] \quad (9)$$

For steady flows, the density on the body is calculated from the equation for total enthalpy, using the computed pressure and velocity, since the freestream stagnation enthalpy H_0 is held constant along the body. For unsteady flows, the density on the body is obtained from extrapolation, since the total enthalpy is not constant along the particle path.

At Upstream and Downstream Boundaries

For subsonic inflow and outflow in the present case, locally one-dimensional Riemann invariants are used at upstream and downstream boundaries. The locally one-dimensional Riemann invariants are given in terms of the normal velocity components and the characteristic velocities $\lambda_1 = V_n$, $\lambda_2 = V_n + a$, and $\lambda_3 = V_n - a$. Two invariants are prescribed at the inlet, and back pressure is imposed at the exit. Other flow variables at the inlet or outlet are calculated by the characteristic equations through iteration.

Results and Discussion

In this study, the channel with length L and a circular-arc throat is chosen. The channel starts at $x = -0.5$ and is terminated at $x = 1.5$; thus, L = 2. The channel throat is located at $x = 0.5$, and the throat area is chosen to be two units (or $h_t/2 = 1$). The imposed back pressure is chosen such that a subsonic inflow passed through the channel and produces a normal shock approximately at the middle (about $x = 0.8$) of the divergent diffuser. The value of parameter τ ranges from 1% to 20%. In order to produce a steady shock wave in the channel, the back pressure chosen for $\tau = 1\%$, 5%, 10%, and 20% are $0.5938P_t$, $0.666P_t$, $0.71P_t$, and $0.712P_t$, respectively, where P_t is the inflow total pressure. Flow unsteadiness is introduced by perturbing the steady back pressure:

$$P_b = P_{b,\,\text{steady}} + \bar{P}\sin[k(t - t_0)] \quad (10)$$

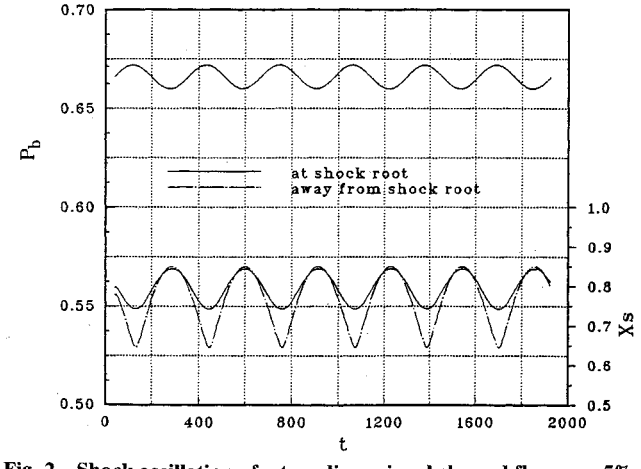

Fig. 2 Shock oscillation of a two-dimensional channel flow, $\tau = 5\%$, $k = 0.01$, and $\bar{P} = 0.006$.

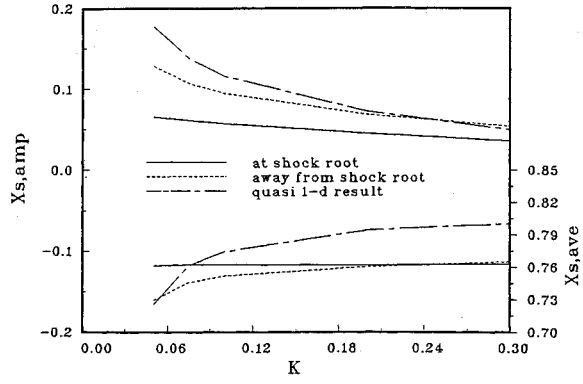

Fig. 3 Variation of average shock position and shock amplitude vs the reduced frequency, $\tau = 10\%$, $\bar{P} = 0.0195$.

where k, $\bar{P}$ are the reduced frequency and amplitude of the imposed pressure, respectively.

The grid used is 60×16 for half computational domain. The Courant number is selected to be 1.5 in order to have a larger time step. All numerical results were performed on a workstation DEC-5000/120.

Shock Movement

A videotape was used in this study to record and observe the shock movement in the channel flow. Figure 2 shows the shock movements at the shock root and at a distance of 0.4 from the wall for $\tau = 5\%$. Similar figures can be obtained for $\tau = 10\%$ and $\tau = 20\%$, which are not shown due to space limitations. It is found that the normal shock does not oscillate uniformly with the same amplitude. The shock amplitude at a distance of 0.4 away from the wall is about 1.8, 2.7, and 2.3 times larger than that at the shock root for $\tau = 5\%$, 10% and $\tau = 20\%$, respectively. Note that for $\tau = 20\%$, the shock amplitude at a distance of 0.6 away from the wall is about 4.2 times larger than that at the shock root. Thus, it is concluded that the amplitude of shock oscillation increases along the shock wave while the shock weakens. Moreover, the amplitude of shock oscillation is greatly influenced by the channel expansion ratio.

The finding that amplitude of shock movement depends on the shock strength was also found in a quasi-one-dimensional channel flow. In this case, two shock waves with the pressure jumps $\Delta P = 0.098$ and 0.16, located initially at $x = 0.725$ and $x = 0.875$, were observed for their movements after the back pressure is perturbed from $P_{b,\,\text{steady}} = 0.67$ and 0.66, respectively. In both cases, k is set to be 0.04. It was found that the amplitude of the weaker shock was about 2.6 times larger than that for the stronger shock.

As reported by Biedron and Adamson,[6] the shock amplitude and the average shock position were linearly proportional to the reduced frequency for pressures at moderate frequencies [$k = \mathcal{O}(1)$]. However, nonlinearity occurred for pressures at low frequencies ($k \ll 1$). Figure 3 shows the shock amplitudes ($X_{s,\,\text{amp}}$) and the average shock positions ($X_{s,\,\text{ave}}$) at the shock root and at a distance of 0.267 from the wall, respectively, at different reduced frequencies for $\tau = 10\%$. It is seen that nonlinearity occurs for $k < 0.21$, and the shock amplitude decreases and the average shock position is moved downstream as the reduced frequency is increased. It is seen that the two-dimensional results are quite different from the quasi-one-dimensional results.

For the channel flow to be in choked conditions, proper values of amplitude and reduced frequency of the perturbed pressure need to be carefully chosen. Namely, there exists an envelope that divides the flow into two regimes: choked and unchoked flows. Numerical calculations indicated that the CPU time needed for the two-dimensional channel flow is about 15 times greater than that for the corresponding quasi-one-dimensional flow. Thus, a quickly obtained envelope in

the amplitude-frequency diagram is presented as a reference for calculation of the two-dimensional flow. Figure 4 shows the envelope of one-dimensional choked flows for $\tau = 1\%$, 5%, and 10%. The envelope for $\tau = 1\%$ is approximated by $\bar{P}_{max} = 0.095k + 0.00135$. Surprisingly, the frequency-amplitude curve for $\tau = 10\%$ is almost linear and parallel to those curves for $\tau = 1\%$ and 5%. Unchoked flows occur in the upper half regions above the straight lines and out on the curves. Since the shock strength becomes weaker away from the shock root and a weaker shock has a larger oscillation amplitude, it is expected that the envelope for a two-dimensional flow would be lower than that for the one-dimensional flow.

The result of Fig. 4 indicates that, for choked flows, the maximum amplitude ($\bar{P}_{max}$) of the imposed fluctuating pressure found for $\tau = 10\%$ is 1.86 times the maximum magnitude for $\tau = 5\%$ thickness wall and 3.21 times that for $\tau = 1\%$. Namely, the choked flow in a channel with larger expansion ratio allows a larger variation in the perturbed pressure. The maximal variation of perturbed pressure found for each case is approximately 3% or less of the steady-state back pressure for the range of k varying from 0.001 to 0.09. One can expect that, for the two-dimensional flows, the allowed maximum disturbance in the imposed pressure would be less than 3%.

Phase Lag

In Ref. 6, Biedron and Adamson found that there existed a phase lag of shock oscillation. It is interesting to know the difference of phase lag between the two-dimensional and corresponding quasi-one-dimensional problems. In the two-dimensional flow, one found the phase lag does not significantly change along the shock wave as the shock amplitude does. Figure 5 shows the comparison of phase lag for the two-dimensional and corresponding one-dimensional flows for different channel expansion ratios. These results indicate that the phase lag in the two-dimensional flow is less serious than (and hence bounded by) that for the one-dimensional flow. Moreover, in the limit of k approaching zero, it appears that there is no phase lag. This limiting result agrees with the result of Biedron and Adamson. Since the CPU time (7 min) needed for the one-dimensional case is much less than that (110 min) for the two-dimensional case, the quasi-one-dimensional flow can provide a quick estimate.

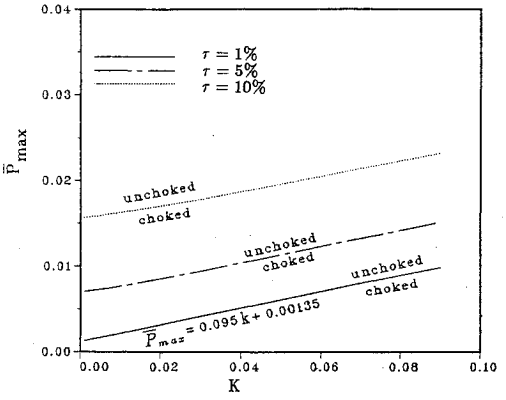

Fig. 4 Envelopes for quasi-one-dimensional flows to be in a choked condition.

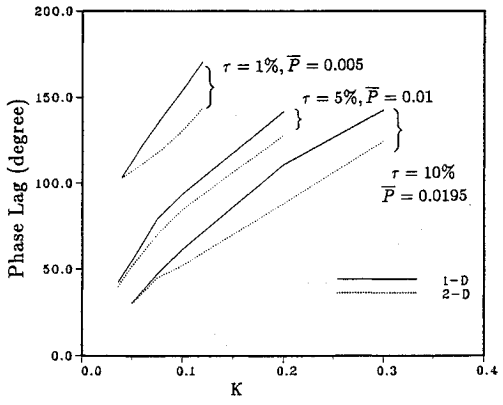

Fig. 5 Comparison of phase lags for two-dimensional and quasi-one-dimensional flows with different channel expansion ratios.

Conclusion

A computational study of two-dimensional forced shock-wave motions in a channel with different expansion ratios is presented. Envelopes for the channel flows to be in a choked condition are shown. The phase lag of shock oscillation found for the two-dimensional flow is limited by that for the corresponding quasi-one-dimensional flow, which provides a fast estimate for engineering application. For choked flows, a channel with larger expansion ratio allows larger variation in the perturbed pressure. The larger the reduced frequency, the smaller the shock amplitude and the farther downstream the average shock position.

Acknowledgments

The support for this study under the contract of the National Science Council, NSC 80-0401-E006-39, and the foreign-university cooperation research fund of the Education Ministry are gratefully acknowledged.

References

[1]Richey, G. K., and Adamson, T. C., Jr., "Analysis of Unsteady Transonic Flow with Shock Waves," *AIAA Journal*, Vol. 14, No. 8, 1976, pp. 1054–1061.

[2]Adamson, T. C., Jr., Messiter, A. F., and Liou, M. S., "Large Amplitude Shock-Wave Motion in Two-Dimensional, Transonic Channel Flows," *AIAA Journal*, Vol. 16, No. 12, 1978, pp. 1240–1247.

[3]Liou, M. S., and Coakley, T. J., "Numerical Simulation of Unsteady Transonic Flow in Diffuser," *AIAA Journal*, Vol. 22, No. 8, 1984, pp. 1139–1145.

[4]Hsieh, T., "Downstream Boundary Effects on the Frequency of Self-Excited Oscillations in Transonic Diffuser," AIAA Paper 87-0161, Reno, NV, Jan. 1987.

[5]Bölcs, A., Fransson, T. H., and Platzer, M. F., "Numerical Simulation of Inviscid Transonic Flow Through Nozzles with Fluctuating Back Pressure," *Journal of Turbomachinery, ASME Transactions*, Vol. 111, April 1989, pp. 169–180.

[6]Biedron, R. T., and Adamson, T. C., Jr., "Unsteady Flow in a Supercritical Supersonic Diffuser," *AIAA Journal*, Vol. 26, No. 11, 1988, pp. 1136–1145.

[7]Liang, S. M., and Tsai, C. J., "Some Insights for Calculations of the Euler Equations" (available from the authors).

[8]Warming, R. F., and Beam, R. M., "On the Construction and Application of Implicit Factored Schemes for Conservation Laws," *SIAM-AMS Proceedings: Computational Fluid Dynamics*, Vol. 11, 1978, pp. 85–129.

[9]Harten, A., "High Resolution Schemes for Hyperbolic Conservation Laws," *Journal of Computational Physics*, Vol. 49, No. 3, 1983, pp. 357–393.

[10]Roe, P. L., "Approximate Riemann Solvers, Parameter Vectors, and Difference Schemes," *Journal of Computational Physics*, Vol. 43, No. 2, 1981, pp. 357–372.

[11]Yee, H. C., "Generalized Formulation of a Class of Explicit and Implicit TVD Schemes," NASA TM-86775, July 1985.

[12]Yee, H. C., "Linearized Form of Implicit TVD Schemes for the Multidimensional Euler and Navier-Stokes Equations," *Computers and Mathematics with Applications*, Vol. 12A, No. 4/5, 1986, pp. 413–432.

[13]Hung, C. M., "Extrapolation of Velocity for Inviscid Solid Boundary Conditions," *AIAA Journal*, Vol. 25, No. 11, 1987, pp. 1513–1515.